

Many-body localization and the area law in two dimensions

K. S. C. Decker^a, D. M. Kennes^{b,c}, and C. Karrasch^{a,1}

^aTechnische Universität Braunschweig, Institut für Mathematische Physik, Mendelssohnstraße 3, 38106 Braunschweig, Germany; ^bInstitut für Theorie der Statistischen Physik, RWTH Aachen University and JARA-Fundamentals of Future Information Technology, 52056 Aachen, Germany; ^cMax Planck Institute for the Structure and Dynamics of Matter, Center for Free-Electron Laser Science, 22761 Hamburg, Germany

This manuscript was compiled on June 25, 2021

We study the high-energy phase diagram of a two-dimensional spin- $\frac{1}{2}$ Heisenberg model on a square lattice in the presence of disorder. The use of large-scale tensor network numerics allows us to compute the bi-partite entanglement entropy for systems of up to 30×7 lattice sites. We demonstrate the existence of a finite many-body localized phase for large disorder strength W for which the eigenstate thermalization hypothesis is violated. Moreover, we show explicitly that the area law holds for excited states in this phase and determine an estimate for the critical W_c where the transition to the ergodic phase occurs.

many-body localization | area law | two dimensions | tensor networks

Paradigmatic to thermodynamics is the assumption that almost any initial state of a generic closed system will evolve into a thermal state governed by the expectation values of a few macroscopic quantities such as energy or particle number (1, 2). Many-body localization (MBL) provides a hallmark exception to this paradigm and generalizes the well-understood phenomena of Anderson localization (3) to the interacting realm. Even in the presence of interactions, too much information of the initial state is retained, which hinders equilibration and the description by a thermal ensemble (4–7). Since the pioneering works of (4, 5), many-body localization has raised tremendous attention as an increasing number of astonishing properties of this phase were uncovered. These include a logarithmic growth of entanglement in quenched systems (8–10), locality of information spread celebrated for potential applications in quantum information sciences (11, 12), unusual transport properties (13–15), and an area law (16) scaling of the entanglement in the *excited states* (17). These findings were substantiated in one spatial dimension by extensive numerical studies that employed mainly exact diagonalization or tensor network approaches as well as the emergence of the so-called ℓ -bit picture (9) which allows the construction of the quasi-local conserved quantities instructively describing the memory of the initial state in the MBL phase (7).

These extensive theoretical efforts were soon complemented by experimental approaches from the field of cold quantum gases (18, 19) or photons (20), which allow an accurate simulation of the thermalization dynamics of quantum many-body systems, or the lack thereof in the case of MBL. Experimental setups are less restrictive in terms of dimensionality, size, time scales, or entanglement growth compared to numerical approaches. They are, however, restricted to studying the evolution of a few initial states, and while quench dynamics can be directly simulated, access to the many-body spectrum – showing many of the prototypical hallmarks of MBL – remains elusive using this experimental route. In addition, experimental setups are not concentrating on quenched but

on quasi-periodic disorder, which is much more convenient to implement.

Taken together, theoretical and experimental advances have significantly deepened our understanding of MBL in one spatial dimensions. First forays into the two-dimensional regime have been undertaken on the level of the quench dynamics, both experimentally (21, 22) and from the numerical point of view (23–26), each with its distinct restrictions. Although some evidence for MBL in two-dimensional systems (27, 28) has recently been accumulated, the state of affairs is much less clear, stimulating a topical debate about whether MBL might ultimately be unstable in two-dimensions (29, 30).

In this work, we employ an accurate numerical approach to establish strong evidence for many-body localization in disordered spin- $\frac{1}{2}$ Heisenberg models on a square lattice. In particular, we show that highly excited eigenstates of the system obey an area law scaling. From the prefactor of this scaling law, we estimate the critical disorder strength where the transition into an ergodic phase occurs and find that it is significantly larger than in the one-dimensional case (23, 31). We also compute the local magnetization and find that it clusters at opposite ends of the fully-polarized spectrum, therefore strongly violating the eigenstate thermalization hypothesis. This clustering weakens with increasing width of the system, which again suggests that the critical strength needed to localize the system strongly increases upon increasing the dimensionality of the system.

Significance Statement

Non-ergodic quantum mechanics cannot be described by a thermal ensemble. Initial states are frozen in time, which can be exploited, e.g., to realize topologically-protected quantum computation away from low temperatures. Quantum systems are, however, typically ergodic. In this work, we use large-scale numerics to demonstrate that a generic two-dimensional lattice of quantum spins exhibits a stable, finite non-ergodic phase. Specifically, we apply a tensor-network approach to study the 2d spin- $\frac{1}{2}$ Heisenberg model. In the presence of sufficiently strong disorder, the system is many-body localized, and the bi-partite entanglement entropy features an area law. We observe a crossover into an ergodic regime as the strength of the disorder decreases.

K.D. performed the numerical calculations. D.M.K. and C.K. interpreted the results and prepared the manuscript.

¹To whom correspondence should be addressed. E-mail: c.karrasch@tu-bs.de

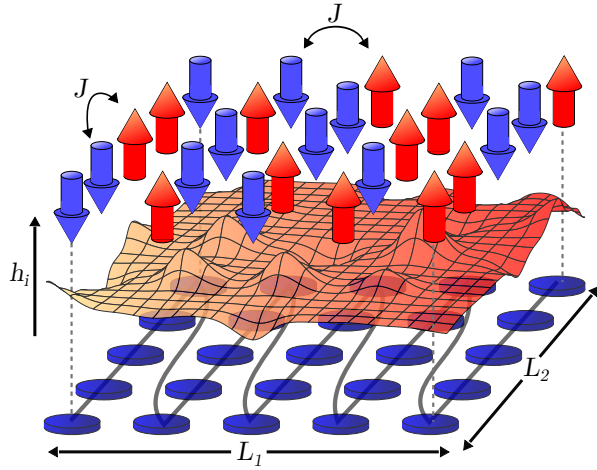


Fig. 1. Sketch of the system studied in this work. Quantum-mechanical spin- $\frac{1}{2}$ degrees of freedom \hat{S}_i are placed on a two-dimensional square lattice of horizontal and vertical dimension L_1 and L_2 , respectively. They interact via a Heisenberg exchange term, see Eq. (1). The strength of the on-site magnetic field h_i fluctuates ('random potential landscape'). The snake-like configuration of the tensor network is indicated at the bottom.

Model and Method. We study the antiferromagnetic Heisenberg model,

$$\hat{H} = J \sum_{\langle i,j \rangle} \hat{S}_i \cdot \hat{S}_j + \sum_i h_i \hat{S}_i^z, \quad [1]$$

where i and j denote nearest neighbors on a two-dimensional square lattice of size $L_1 \times L_2$, and $\hat{S}_i = (\hat{S}_i^x, \hat{S}_i^y, \hat{S}_i^z)^T$ is a quantum-mechanical spin- $\frac{1}{2}$ degree of freedom. The on-site magnetic fields h_i are drawn randomly from a uniform distribution $[-W, W]$. All results are averaged over 1000 different disorder realizations. From now on, we set $J = 1$ as the unit of energy. In the vertical direction associated with L_2 , we employ either open (or cylindric boundary conditions (OBC or CBC); the system always has open boundaries in the horizontal direction associated with L_1 . Our setup is illustrated in Fig. 1.

We determine a random excited eigenstate – which is generically a high-energy, mid-spectrum state – of the Hamiltonian in Eq. (1) using the density-matrix renormalization group (DMRG). The DMRG is an accurate, tensor-network based method to study quantum systems (32–34) which was originally devised to compute ground states in one dimension but was later extended to tackle 2d problems (35, 36) as well as excited states in problems with disorder (37–40). In this paper, we combine these developments and for the first time investigate high-energy states in a 2d system using the DMRG-X technique (37). The key numerical control parameter is the so-called local bond dimension χ , which is a measure of the amount of entanglement in the system. We work with a maximum value of $\chi = 64$, which is sufficient to obtain results that are exact up to machine precision for almost all parameters. More details can be found in the ‘Materials and Methods’ section (see in particular Fig. 5).

Results. We first study the von Neumann entropy,

$$S_{vN} = -\text{tr} \hat{\rho} \log_2 \hat{\rho}, \quad [2]$$

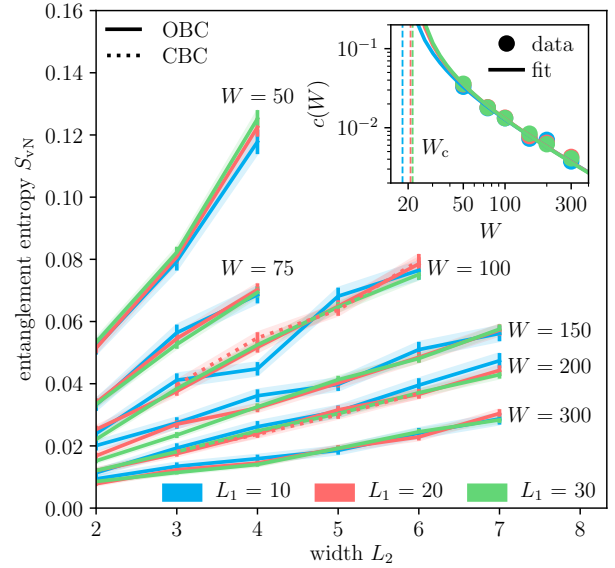


Fig. 2. The bi-partite entanglement entropy of high-energy eigenstates of a lattice of length L_1 and width L_2 is computed using tensor networks for various disorder strengths W and different boundary conditions. The system is cut vertically around the middle (see Fig. 3 for details), and S_{vN} grows linearly with L_2 but is independent of L_1 . This demonstrates the entanglement area law. The vertical lines indicate the error associated with the disorder averaging. *Inset:* Proportionality constant $c(W)$ in $S_{vN} = c(W)L_2$. A divergence at a critical value W_c signals the crossover into an ergodic phase.

where $\hat{\rho}$ is the reduced density matrix of one half of a system that is cut vertically. This is a measure of the *bi-partite entanglement*. In a thermal ensemble, S_{vN} is an extensive quantity that should scale with the volume $L_1 L_2$ of the system. Due to the eigenstate thermalization hypothesis, the same should hold true for an eigenstate whose local properties are reflective of the thermal ones at the corresponding energy. The behavior of a localized state, however, is very different: the area law stipulates that S_{vN} is independent of L_1 but increases linearly with L_2 , i.e., with the area between both halves of the bi-partition. The entanglement entropy can thus be used to differentiate between those two phases of matter.

In Fig. 2, we show S_{vN} as a function of L_2 for various L_1 , different disorder strengths W , and for both open and cylindric boundary conditions (note that CBC data is only included for $L_1 = 20, L_2 \leq 6, W \in \{75, 100\}$). We averaged over all vertical cuts in the middle area of the system, which we defined as $\pm 20\%$ around the center (our results do not depend on this precise choice, see Fig. 3). One observes that the entanglement entropy does not depend on L_1 but scales linearly with L_2 . This clearly demonstrates the area law and the existence of a many-body localized phase of the two-dimensional Heisenberg model at sufficiently large W .

As the strength of the disorder decreases, the entanglement entropy grows, and eventually the local bond dimension and thus the numerical effort become prohibitively large. This can be quantified by studying the prefactor $c(W)$ appearing in the area law, $S_{vN} = c(W)L_2$, which is plotted in the inset to Fig. 2. The raw data is fitted to the functional form $c(W) = a/(W - W_c)$. From this analysis, one estimates that the transition into the ergodic phase occurs at around $W_c \approx 20$. This value of W_c is in good agreement with ℓ -

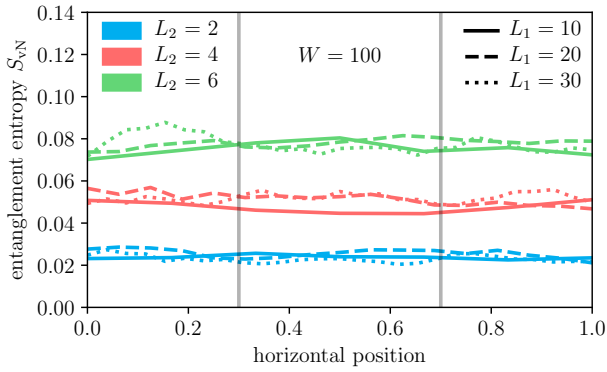


Fig. 3. Bi-partite entanglement entropy as a function of the relative horizontal position where the lattice is cut vertically for various values of L_1 and L_2 . The area law stipulates that $S_{vN} \sim L_2$ while being independent of L_1 . We show a running average over three neighboring data points. The gray lines indicate the ‘middle area’ whose average value is plotted in Fig. 2.

bit studies of the same system (27, 28). Importantly, this transition point is extracted directly from the area law scaling of the entanglement, a prototypical feature of many-body localization.

Another hallmark of the localized phase is the lack of ergodicity. In an ergodic system, the eigenstate thermalization hypothesis dictates that local properties of generic eigenstates mirror the behavior of a thermal ensemble. In the left column of Fig. 4, we plot the distribution of the local magnetization $\langle 2\hat{S}_i^z \rangle$ for all sites i , fixed L_1 , W , and various L_2 . We do not observe a thermal peak at $\langle 2\hat{S}_i^z \rangle = 0$ but a strong pinning around $\langle 2\hat{S}_i^z \rangle = \pm 1$. Overall the distribution is symmetric around $\langle 2\hat{S}_i^z \rangle = 0$. This illustrates that the eigenstate thermalization hypothesis is prominently violated and that the system is localized. To quantify the strength of the pinning to $\langle 2\hat{S}_i^z \rangle = \pm 1$ and thus non-ergodicity in the MBL phase more clearly, we plot in the right column of Fig. 4 the fraction of the spectrum of $|\langle 2\hat{S}_i^z \rangle|$ that lies below a given threshold. Varying the threshold from 0 to 1 (which correspond to the middle and the ends of the spectrum of $\langle 2\hat{S}_i^z \rangle$, respectively) we find that only extremely little weight (less than 10%) does lie within a window of 5% around the ends of the spectrum. Furthermore, the growth of weight as one approaches the end of the spectrum is faster than exponential, underlining the extreme pinning of the expectation values of the local spins to $\langle 2\hat{S}_i^z \rangle = \pm 1$.

Discussion. Our findings provide further evidence for many-body localization of systems in higher than one dimension. In particular, we studied the behavior of the entanglement entropy as the two-dimensional limit is approached and established a rigorous area law scaling as L_2 is increased at fixed $L_1 > L_2$. We employed an accurate tensor-network based method that circumvents most of the criticism applicable to other approaches such as weak coupling expansions or approximate effective representations like the ℓ -bit picture, which are very powerful but hard to converge in two dimensions. It is often argued that ultimately many-body localization is unstable in higher than one dimension, which can now be further refuted due to our findings.

The area law in localized systems renders them an ideal playground for a tensor-network approach whose accuracy

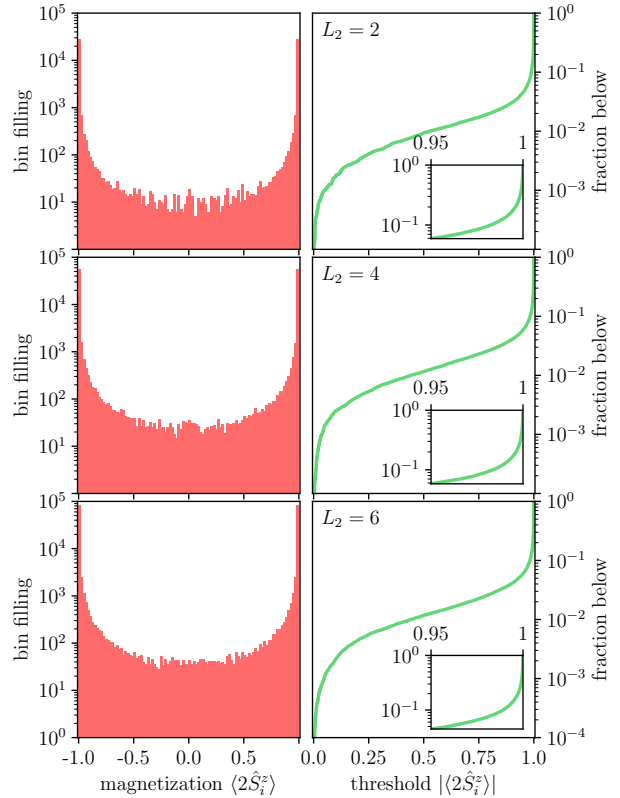


Fig. 4. Distribution of the magnetization $\langle 2\hat{S}_i^z \rangle$ in high-energy eigenstates for $L_1 = 30$, different L_2 , and $W = 100$. Due to the lack of ergodicity, the eigenstate thermalization hypothesis is violated. We do not observe a peak at $\langle 2\hat{S}_i^z \rangle = 0$ but a strong pinning around $\langle 2\hat{S}_i^z \rangle = \pm 1$. This is illustrated more clearly by plotting the fraction of values $|\langle 2\hat{S}_i^z \rangle|$ that lie below a given threshold.

and complexity grows with the amount of entanglement in the system. However, the numerical effort is still substantial, since the complexity to capture an area-law in two dimensions roughly corresponds to the one of a volume law in 1d. On the other hand, the amount of entanglement decreases with the strength of the disorder, and a ‘sweet spot’ can be found trading disorder strength for system size. By exploring the scaling with respect to system size at this sweet spot, we can extrapolate a finite critical disorder strength where the transition to the ergodic phase occurs and as a consequence rigorously establish many-body localization in two dimensions.

The methodology put forward in this work can be applied straightforwardly to other systems such as those subject to a quasi-periodic instead of a random potential, which are currently in the experimental focus. Future investigation could point out similarities and possibly differences of many-body localization in varying dimensions, e.g., the transport behavior and the perspective of MBL in 2d for the imminent age of noisy intermediate-scale quantum computing (41, 42). Finally, if two dimensions are not enough to suppress the presence of a many-body localized regime, it begs the question: Is there a finite dimensionality d_c at which MBL indeed will be unstable?

Materials and Methods

In a one-dimensional system of size L , any state can be expressed

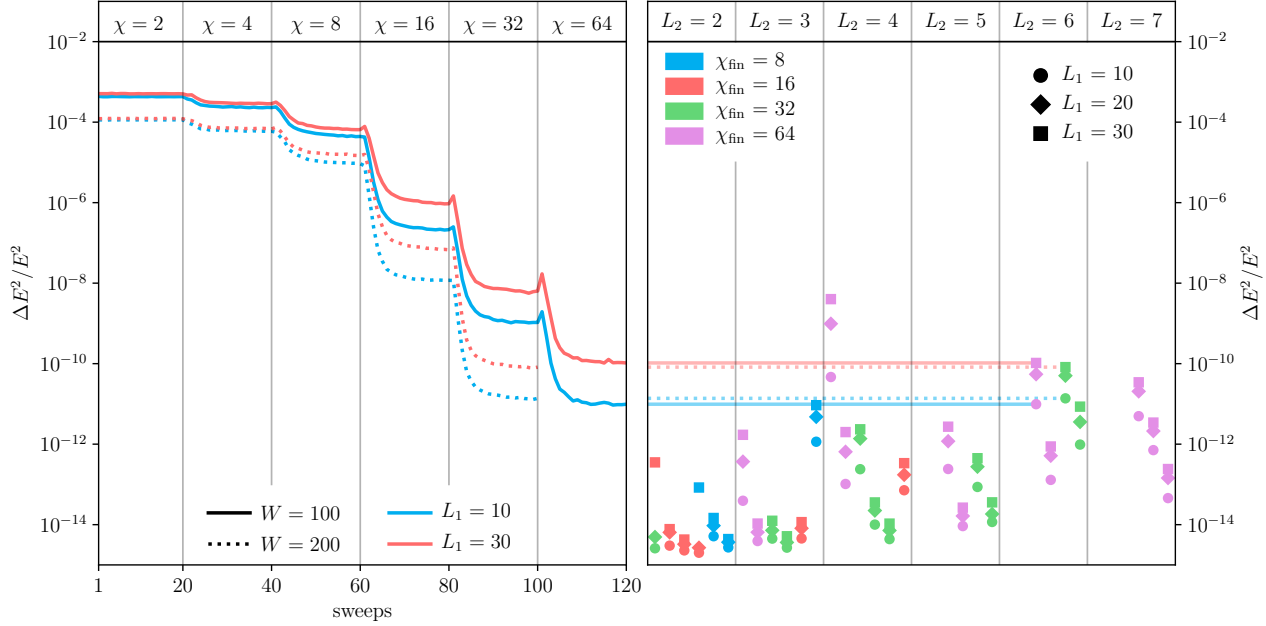


Fig. 5. *Left panel:* Rescaled energy variance $\Delta E/E^2$ of high-energy eigenstates as a function of the DMRG-X sweeps for a system of length $L_1 \in \{10, 30\}$, width $L_2 = 6$, and open boundary conditions for two different disorder strengths $W \in \{100, 200\}$. The local bond dimension χ is successively increased until $\Delta E/E^2$ has sufficiently converged. By exploiting $U(1)$ symmetries, we can work with values as large as $\chi = 64$. *Right panel:* Scatter plot of the energy variance at the end of the DMRG-X sweeping procedure. The individual data points correspond to all parameter sets $\{L_1, L_2, W\}$ shown in Fig. 2. For fixed L_2 , the disorder strength W increases from left to right. The different colors indicate the *final* value of the local bond dimension for the corresponding parameters. The solid and dashed lines illustrate which data points correspond to the four parameter sets shown in the left panel.

in terms of a matrix-product state,

$$|\Psi\rangle = \sum_{\{\sigma_i\}} \text{tr}(A^{\sigma_1} \cdots A^{\sigma_L}) |\sigma_1 \cdots \sigma_L\rangle, \quad [3]$$

where σ_i denotes a local basis such as the eigenbasis of \hat{S}_i^z . The maximum size χ of the matrices A^{σ_i} is called the local bond dimension and encodes the amount of entanglement in the state.

We employ the so-called DMRG-X technique to determine a highly-excited eigenstate of the Hamiltonian in Eq. (1). The key idea is to start out in a random product state that is an eigenstate of $\hat{\mathcal{H}}$ in the limit of large h_i . Thereafter, the matrices A^{σ_i} are updated successively from left to right (and vice versa) by so-called DMRG sweeps. In contrast to a variational ground state calculation, we do not choose the lowest-energy state during each update but pick the state which has maximum overlap with the prior one (37). This accounts for the fact that localized eigenstates which have similar energy differ vastly in their spatial structures.

The local bond dimension χ is successively increased after each 20 sweeps (see the left panel of Fig. 5). The calculation is stopped whenever the rescaled energy variance has sufficiently converged. By implementing the DMRG-X approach using $U(1)$ -symmetries, we can reach a maximum value of $\chi = 64$. This allows us to obtain eigenstates with an energy variance close to machine precision for almost all parameter sets $\{L_1, L_2, W\}$ shown in this paper (see the right panel of Fig. 5).

In order to apply the DMRG-X, our two-dimensional lattice is first transformed into a one-dimensional chain in a snake-like fashion (see Fig. 1). Due to this mapping, the Hamiltonian contains long-range terms. We choose a scheme where the snake connects the bottom of each column to the top of the next column, which has the distinct advantage that the local bond dimension of the matrix product operator that represents $\hat{\mathcal{H}}$, which scales linearly with L_2 , is reduced compared to the standard approach where subsequent columns are traversed in the opposite order.

ACKNOWLEDGMENTS. K.D. and C.K. acknowledge support by the Deutsche Forschungsgemeinschaft (DFG, German Research

Foundation) through the Emmy Noether program (KA3360/2-1) as well as by ‘Niedersächsisches Vorab’ through the ‘Quantum- and Nano-Metrology (QUANOMET)’ initiative within the project P-1. D.M.K. was supported by the Deutsche Forschungsgemeinschaft (DFG, German Research Foundation) via Germany’s Excellence Strategy – Cluster of Excellence Matter and Light for Quantum Computing (ML4Q) EXC 2004/1 – 390534769. We acknowledge support from the Max Planck-New York City Center for Non-Equilibrium Quantum Phenomena.

While writing up this manuscript, Ref. (43) appeared which analyzes a similar question but with a different focus and methodology.

- Polkovnikov A, Sengupta K, Silva A, Vengalattore M (2011) Colloquium: Nonequilibrium dynamics of closed interacting quantum systems. *Rev. Mod. Phys.* 83(3):863–883.
- Gogolin C, Eisert J (2016) Equilibration, thermalisation, and the emergence of statistical mechanics in closed quantum systems. *Reports on Progress in Physics* 79(5):056001.
- Anderson PW (1958) Absence of diffusion in certain random lattices. *Phys. Rev.* 109(5):1492–1505.
- Gornyi IV, Mirlin AD, Polyakov DG (2005) Interacting electrons in disordered wires: Anderson localization and low- t transport. *Phys. Rev. Lett.* 95(20):206603.
- Basko DM, Aleiner IL, Altshuler BL (2006) Metal-insulator transition in a weakly interacting many-electron system with localized single-particle states. *Ann. Phys.* 321:1126.
- Pal A, Huse DA (2010) Many-body localization phase transition. *Phys. Rev. B* 82(17):174411.
- Abanin DA, Altman E, Bloch I, Serbyn M (2019) Colloquium: Many-body localization, thermalization, and entanglement. *Rev. Mod. Phys.* 91(2):021001.
- Bardarson JH, Pollmann F, Moore JE (2012) Unbounded growth of entanglement in models of many-body localization. *Phys. Rev. Lett.* 109(1):017202.
- Serbyn M, Papić Z, Abanin DA (2013) Universal slow growth of entanglement in interacting strongly disordered systems. *Phys. Rev. Lett.* 110(26):260601.
- Žnidarič M, Prosen Tcv, Prelovšek P (2008) Many-body localization in the heisenberg xxx magnet in a random field. *Phys. Rev. B* 77(6):064426.
- Bañuls MC, Yao NY, Choi S, Lukin MD, Cirac JI (2017) Dynamics of quantum information in many-body localized systems. *Phys. Rev. B* 96(17):174201.
- Friedsdorf M, Werner AH, Gohl M, Eisert J, Brown W (2015) Local constants of motion imply information propagation. *New Journal of Physics* 17(11):113054.
- Luitz DJ, Lev YB (2017) The ergodic side of the many-body localization transition. *Annalen der Physik* 529(7):1600350.
- Agarwal K, et al. (2017) Rare-region effects and dynamics near the many-body localization transition. *Annalen der Physik* 529(7):1600326.
- Lev YB, Kennes DM, Klöckner C, Reichman DF, Karrasch C (2017) Transport in quasisperi-

- odic interacting systems: From superdiffusion to subdiffusion. *EPL (Europhysics Letters)* 119(3):37003.
16. Eisert J, Cramer M, Plenio MB (2010) Colloquium: Area laws for the entanglement entropy. *Rev. Mod. Phys.* 82(1):277–306.
 17. Bauer B, Nayak C (2013) Area laws in a many-body localized state and its implications for topological order. *Journal of Statistical Mechanics: Theory and Experiment* 2013(09):P09005.
 18. Schreiber M, et al. (2015) Observation of many-body localization of interacting fermions in a quasirandom optical lattice. *Science* 349(6250):842–845.
 19. Smith J, et al. (2016) Many-body localization in a quantum simulator with programmable random disorder. *Nature Physics* 12(10):907–911.
 20. Roushan P, et al. (2017) Spectroscopic signatures of localization with interacting photons in superconducting qubits. *Science* 358(6367):1175–1179.
 21. Choi Jy, et al. (2016) Exploring the many-body localization transition in two dimensions. *Science* 352(6293):1547–1552.
 22. Bordia P, et al. (2017) Probing slow relaxation and many-body localization in two-dimensional quasiperiodic systems. *Phys. Rev. X* 7(4):041047.
 23. Kennes DM (2018) Many-body localization in two dimensions from projected entangled-pair states. *arXiv:1811.04126*.
 24. Hubig C, Cirac JI (2019) Time-dependent study of disordered models with infinite projected entangled pair states. *SciPost Phys.* 6(3):31.
 25. De Tomasi G, Pollmann F, Heyl M (2019) Efficiently solving the dynamics of many-body localized systems at strong disorder. *Phys. Rev. B* 99(24):241114.
 26. Kshetrimayum A, Goihl M, Eisert J (2020) Time evolution of many-body localized systems in two spatial dimensions. *Phys. Rev. B* 102(23):235132.
 27. Wahl TB, Pal A, Simon SH (2019) Signatures of the many-body localized regime in two dimensions. *Nature Physics* 15(2):164–169.
 28. Chertkov E, Villalonga B, Clark BK (2021) Numerical evidence for many-body localization in two and three dimensions. *Phys. Rev. Lett.* 126(18):180602.
 29. De Roeck W, Huveneers Fmc (2017) Stability and instability towards delocalization in many-body localization systems. *Phys. Rev. B* 95(15):155129.
 30. De Roeck W, Imbrie JZ (2017) Many-body localization: stability and instability. *Philosophical Transactions of the Royal Society A: Mathematical, Physical and Engineering Sciences* 375(2108):20160422.
 31. Luitz DJ, Laflorencie N, Alet F (2015) Many-body localization edge in the random-field heisenberg chain. *Phys. Rev. B* 91(8):081103.
 32. White SR (1992) Density matrix formulation for quantum renormalization groups. *Phys. Rev. Lett.* 69(19):2863–2866.
 33. Schollwöck U (2005) The density-matrix renormalization group. *Rev. Mod. Phys.* 77(1):259–315.
 34. Schollwöck U (2011) The density-matrix renormalization group in the age of matrix product states. *Annals of Physics* 326(1):96–192.
 35. Stoudenmire E, White SR (2012) Studying two-dimensional systems with the density matrix renormalization group. *Annual Review of Condensed Matter Physics* 3(1):111–128.
 36. Hyatt K, Stoudenmire EM (2020) DMRG Approach to Optimizing Two-Dimensional Tensor Networks. *arXiv:1908.08833v2*.
 37. Khemani V, Pollmann F, Sondhi SL (2016) Obtaining highly excited eigenstates of many-body localized hamiltonians by the density matrix renormalization group approach. *Phys. Rev. Lett.* 116(24):247204.
 38. Lim SP, Sheng DN (2016) Many-body localization and transition by density matrix renormalization group and exact diagonalization studies. *Phys. Rev. B* 94(4):045111.
 39. Kennes DM, Karrasch C (2016) Entanglement scaling of excited states in large one-dimensional many-body localized systems. *Phys. Rev. B* 93(24):245129.
 40. Yu X, Pekker D, Clark BK (2017) Finding matrix product state representations of highly excited eigenstates of many-body localized hamiltonians. *Phys. Rev. Lett.* 118(1):017201.
 41. Preskill J (2018) Quantum Computing in the NISQ era and beyond. *Quantum* 2:79.
 42. Kshetrimayum A, Goihl M, Kennes DM, Eisert J (2021) Quantum time crystals with programmable disorder in higher dimensions. *Phys. Rev. B* 103(22):224205.
 43. Tang HK, et al. (2021) Evidence of many-body localization in 2d from quantum monte carlo simulation. *arXiv:2106.08587*.